Design Swelling Micas: Insights on Heavy Metals Cation Exchange Reaction.

Francisco J. Osuna[1], Esperanza Pavón[1], María D. Alba[1,*]

[1]Instituto Ciencia de los Materiales de Sevilla (CSIC-US). Avda. Américo Vespucio, 49. 41092-Sevilla, Spain

ABSTRACT

Heavy metal pollution has become one of the most serious environmental problems, demanding specialized remediation mechanisms. Among the studied treatments, ion-exchange processes have been widely used due to their high remediation capacity, efficiency and fast kinetic. Here, the potential use of a new family of design micas as cation exchanger has been analysed. Micas with a layer charge in the range of brittle micas have been synthesized and their heavy metals cation exchange capacity analysed as a function of the nature of the heavy metal cations (Pb^{2+}, Cd^{2+} or Hg^{2+}), the nature of the counterions (Cl^- or NO_3^-), concentration of the solutions and the micas layer charge. A cation exchange ratio between 35 % and 154 % of their cation exchange capacity (*CEC*) was achieved, being more efficient when mica layer charge diminished. In general, the maximum adsorption capacity followed the trend: $Hg^{2+} > Pb^{2+} > Cd^{2+}$. The efficiency of the cation exchange and adsorption mechanism of the synthetic micas depended on the experimental conditions and they were more efficient than raw and modified natural clay minerals.

Keywords. heavy metals; hazardous materials; design clay; cation exchange capacity.

* Corresponding author: alba@icmse.csic.es

1. Introduction

Heavy metal pollution has become one of the most serious environmental problems. Zinc, copper, nickel, mercury, cadmium, lead and chromium are the most hazardous heavy metals and, consequently, they are of particular concern in the treatment of industrial wastewaters, due to their recalcitrance and persistence in the environment. In recent years, various methods for heavy metal removal from wastewater have been extensively studied (Fu and Wang, 2011). Among them, ion-exchange processes have been widely used due to their high treatment capacity, high removal efficiency and fast kinetic (Kang et al., 2004).

Among the most used materials for ionic exchange, clay minerals and their derivatives are drawing wide concerns nowadays, differing from other materials such as activated carbon, zeolite, and resin in terms of the microstructure, adsorptive characteristics, and environmental applications (Churchman et al., 2006; Yuan, 2004; Yuan et al., 2013; Zhu et al., 2015). However, their use is still limited compared with synthetic resins and more research is needed for their application at an industrial scale and the use of alternative low-cost adsorbent materials have been emphasized.

The adsorption capacity of the natural clay minerals is quite limited (Syrmanova et al., 2016), thus, many studies have been devoted to enhance their metal uptake (Jimenez-Castaneda and Medina, 2017; O'Connell et al., 2008; Srinivasan, 2011). In his sense, Alba et al. (Alba et al., 2006) have synthetized a new family of the swelling high charged fluorophlogopite, with layer charge in the range of the brittle micas (Pavon et al., 2014) but unlike the natural micas, they exhibit swelling properties and cation exchange capacity (Pavon et al., 2013). Those synthetic micas, Na-M*n* (*n* is the layer charge ranging between 2 and 4), have exhibited excellent capacity for radioactive cations and organic

pollutants removal from wastewater (Alba et al., 2006; Garcia-Jimenez et al., 2016; Pazos et al., 2017) and are promising materials for heavy metal ion-exchange processes. Moreover, the use of synthetic samples is a potentially useful alternative for a proper understanding of the physical chemistry of the ion exchange reaction.

The present work provides basic and extensive information on cation exchange for divalent heavy metals cations as a function of structural parameters of the micas (layer charge) and experimental conditions such as nature of the heavy metals (Pb^{2+}, Cd^{2+} or Hg^{2+}, which even in very low levels cause neurological, reproductive, cardiovascular, and developmental damage (Al-Saleh et al., 2008; Kim et al., 2012)), the counterions nature (Cl^- or NO_3^-) or initial solution concentration. All the experimental variables have been summarized in Table 1.

2. Experimental

2.1. Materials

Na-M*n* (*n* is the layer charge equals to 2 or 4) were synthetized by mixing SiO_2, Al_2O_3, MgF_2, and NaCl in the molar ratio 8-*n*:*n*:6:2*n*. The starting materials were SiO_2 from Sigma (CAS no. 112945-52-5, 99.8% purity), $Al(OH)_3$ from Sigma Aldrich (CAS no. 21645-51-2, 99% purity), MgF_2 from Aldrich (CAS no. 20831-0, 98% purity), and NaCl from Panreac (CAS no. 131659, 99.5% purity). All reagents were mixed and ground in an agate mortar and, then, were heated up to 900 °C for 15 h in a Pt crucible. Finally, the solids were washed with deionized water and dried at room temperature (Alba et al., 2006).

2.2. Cation Exchange reaction

The as-synthetized samples were equilibrated with solutions of Pb^{2+}, Cd^{2+} and Hg^{2+}, following the methodology described by Pavon el at. (Pavon et al., 2013). The most important characteristics of these ions in solutions are displayed in Table 2 (Gonzalez-Davila et al., 2007; Matusik and Wscislo, 2014; Pearson, 1988; Persson, 2010). Different parameters were tested in the equilibrium reaction in order to analyse the influence of each one (Table 1): initial solution concentration (Samples A *vs* Sample B), the nature of the counterion (Cl^- or NO_3^-, Samples B vs C), stirring (Samples C vs D) and mica layer charge (Samples D). 500 mg of solid were used and the reaction took place at 25 ºC during 24 h, previous studies demonstrated that the equilibrium should be reached at this time (Kodama et al., 2000; Kodama et al., 2004). To avoid the hydrolysis of cations in the solution and the precipitation of metal hydroxides and oxides, the *pH* of the solutions were previously set below 6 for Pb^{2+} and Cd^{2+} and below 2.5 for Hg^{2+} (Table S1 and Fig. S1) (Uddin, 2017). After equilibration, the solutions were centrifuged at 10000 rpm for 20 min. The whole equilibrium reaction with fresh solution and phase separation were repeated three more times. In all the cases, the solids were later washed with milli-Q water for four times.

The *pH* and potential (E_H) values of the supernatants were measured (Table S1 and Fig. S1) and, then, they were kept under acid and freezing conditions. The solids were dried at room temperature and grinded afterwards.

2.3. Characterization

ICP-AES (Inductively Coupled Plasma-Atomic Emission Spectrometry) was used to analyse the metal content on the initial solutions and the supernatants obtained after the equilibrium reactions. Measurements were carried out at microanalysis laboratory

(CITIUS, University of Seville, Spain) using a HORIBA JOBIN YVON-ULTIMA 2 equipment.

Powder X-ray diffraction (XRD) was carried out to check the phase purity, to determine the basal spacing of the micas, and to monitor crystallinity. XRD patterns were obtained at the X-ray laboratory (CITIUS, University of Seville, Spain) on a Bruker D8 Advance instrument equipped with a Cu K_α radiation source operating at 40 kV and 40 mA. Diffractograms were obtained in the 2θ range of 3–70° with a step size of 0.015° and a step time of 0.1 s.

Scanning electron microscopy (SEM/EDX) was used to determine particle size, shape and elemental composition of particles. The images were recorded at 20 kV in the Microscopy Service of ICMS (CSIC-US) using a JEOL Model JSM 5400. An EDX system (Oxford Link ISIS) was fitted to the SEM equipment to perform chemical analyses of the sample using a Si/Li detector with Be window.

Solid state nuclear magnetic resonance (MAS-NMR) was used to analyse the local order of the framework heteroatoms (^{29}Si and ^{27}Al MAS NMR) and the evolution of the sodium in the interlayer space (^{23}Na MAS NMR). Single-pulse (SP) MAS-NMR experiments were recorded on a Bruker AVANCE WB400 spectrometer equipped with a multinuclear probe, at the Nuclear Magnetic Resonance Service of University of Córdoba (Córdoba, Spain). Powdered samples were packed in 3.2 mm zirconia rotors and spun at 10 kHz. ^{29}Si MAS-NMR spectra were acquired at a frequency of 79.49 MHz, pulse width of 2.7 μs (π/6) each 3 s. ^{27}Al MAS-NMR spectra were recorded at 104.26 MHz with a pulse of 0.38 μs (π/20) and a delay time of 0.5 s. ^{23}Na MAS NMR spectrum was recorded at 105.84 MHz with a pulse width of 0.75 μs (π/2 pulse length = 4.5 μs) and a delay time of 0.1 s. The chemical shift values were reported in ppm from tetramethylsilane for ^{29}Si and from a 0.1 M $AlCl_3$ and NaCl solution for ^{27}Al and ^{23}Na, respectively.

3. Results and discussion

The amount of desorbed sodium (C_{ds}) and adsorbed heavy metals (C_s) in Na-M4 samples were below its cation exchange capacity (Fig. 1). Two reasons can explain this behaviour: i) an equilibrium state between the cations in the mica interlayer space and those in solution: Na-M4 (s) + X^{2+} (aq) = Na/X-M4 (s) + Na^+/X^{2+}(aq), ii) a partial compensation of the layer charge by hydronium ions from the hydrolysis of the heavy metal cations in aqueous solution, and/or, iii) cations leached from the mica framework due to the acid medium.

In Na-M4, Na^+ was not completely desorbed and X^{2+} was adsorbed below the *CEC* (Fig. 1), which indicates that beside cationic exchange reaction other mechanisms are involved in the adsorption. The only exceptions are samples Hg-M4-A and Hg-M4-D where it is below the *CEC* probably due to a partial compensation of the layer charge by H_3O^+ ions (Park et al., 2012) or leached framework cations to the interlayer space (Alba et al., 2001a, b).

For Na-M2, Pb^{2+} and Cd^{2+} are adsorbed above its *CEC* although Na^+ is not completely desorbed whereas Hg^{2+} absorption is 76 % of its *CEC* and Na^+ is completely desorbed (Fig. 1). In the former, both cation exchange and precipitation are the mechanisms for the metal absorption. Hg^{2+} cation is more easily hydrolysable in aqueous solution than Pb^{2+} and Cd^{2+} (pK_H=3.4 (Gonzalez-Davila et al., 2007) vs the pK_H= 7.7. or 10.1 for Pb^{2+} and Cd^{2+} (Matusik and Wscislo, 2014), Table 2, then, in the Hg^{2+} exchange reaction, a partial compensation of the layer charge may occur due to H_3O^+ ions (Park et al., 2012).

The XRD peak for *001* reflection remains strong for the divalent metal exchanged micas (Fig. 2) and the basal spacing ranges from 1.21 to 1.39 nm indicating that, after the

exchange, the interlayer structure of the hydrated micas is retained as a single water sheet or double sheet of interlayer cation, respectively (Kodama and Komarneni, 1999).

Intercalated divalent cations influence the electrostatic attraction, which can be explained by cation hardness (η). As previously reported for rare-earth cations (Takahashi et al., 2004), the interaction between interlayer cations and montmorillonite surface is favoured for hard cations. When the η for the interlayer cations is high as Cd^{2+}, 10.29, (Pearson, 1988) a unique *001* reflection at ca. 1.21 nm, corresponding to a similar hydration state to Na^{+} in Na-M4, is observed. In contrast, when the η ratio of the interlayer cations is low, as Pb^{2+} and Hg^{2+}, 8.46 and 7.7 respectively, (Pearson, 1988) a more complex behaviour, with additional *001* reflections at high basal space, is observed. Higher basal space is observed for Hg-M4-A and Hg-M4-B than for Pb-M4-A and Pb-M4-B, in good agreement with their respectively hardness (Fig. 2).

Besides the mica structure and depending on the experiment, new crystalline phases are detected by XRD (Fig. 2), except for the Cd^{2+} samples that the mica phase remain unaltered. In Pb-M4-A and Pb-M4-B, where the *pH* of initial solution was quite low, crystalline spinel is formed together with $PbCl_2$ whereas in Pb-M4-C and D, lead oxide and fluorine are observed. In Hg-M4-C and Hg-M4-D, two crystalline phases containing Mg and/or Si are detected. HgO and $Hg(NO_3)_3$ crystalline phases are also observed in Hg-M4-C.

Scanning electron micrographs of all samples indicate that the morphology is not affected by the cation exchange reaction (figures non shown). However, the elemental composition of the layer changes with the experimental conditions (Fig. S2). After the exchange reactions, the intensity of Na K_α line diminishes and new lines representative of the heavy metal increases as expected from the elemental analysis results. On the other

hand, the intensity of the framework Si, Al and Mg K_α lines changes depending on the experimental conditions.

It is remarkable, the absence of the Hg M line in the EDX spectra of Hg-M4-A and Hg-M4-B (Fig. S2) although Na^+ was desorbed and Hg^{2+} was adsorbed (Fig. 1). This fact remarks that Na^+ could be exchanged by H_3O^+ due to Hg^{2+}/Hg_2^{2+} hydrolysis or to framework cations leached in the acidic reaction medium (Table S1).

^{23}Na MAS NMR spectra of Na-M*n* (*n*=2 and 4) (Fig. 3) are characterized by a broad signal between 10 and -30 ppm due to exchangeable hydrated cation and, in the case of Na-M2, an additional peak at ca. 37 ppm due to non-exchangeable Na^+ is also observed (Naranjo et al., 2015). After the metal exchange reaction, the intensity of the exchangeable Na^+ signal decreases in good agreement with the quantity of remainder sodium after the exchange reaction (Fig. 1) and the intensity of the non-exchangeable ^{23}Na NMR signal of the X-M2-D (X=Pb^{2+} and Cd^{2+}) spectra remains constant. Especial attention demands the ^{23}Na MAS NMR spectrum of Hg-M2-D, the signal of the exchangeable hydrated cation (between 10 to -30 ppm) disappears and the intensity of the signal at ca. 37 ppm decreases. The Na^+ desorbed by Hg-M2-D is slightly higher than their *CEC* and it could account not only the exchangeable interlayer Na^+ but also part of non-exchangeable Na^+ that was leached in an acidic medium (Table S1) as pointed by ^{23}Na MAS NMR.

^{27}Al MAS NMR spectra (Fig. S3) show an asymmetric band at ca. 67 ppm corresponding to Al^{3+} in tetrahedral coordination (Sanz and Serratosa, 1984). The ^{27}Al MAS NMR spectrum for Na-M2 (Fig. S3) shows only this Al resonance at 67.3 ppm, indicating the presence of only tetrahedral Al^{3+}, while Na-M4 (Fig. S3) has small amounts of octahedral coordinated Al^{3+} in Mg^{2+} trioctahedral sheets resonating at ca. 0 ppm.

However, most of the Al^{3+} atoms are predominantly present in tetrahedral sheet as evidenced by the very strong tetrahedral Al^{3+} resonance at 68.5 ppm.

After cation-exchange reaction, a broadening of the ^{27}Al signals is observed, due to the distortion exerted on the tetrahedral Al^{3+} as consequence of the location of the interlayer cation in the pseudohexagonal cavity (Alvero et al., 1994). The exchange with Hg^{2+} also provokes an increasing in the octahedral ^{27}Al signal in Hg-M4, due to the leached Al^{3+} as consequence of the low *pH* value of the initial solution (Table S1). Part of this Al^{3+} could be responsible of satisfying the total *CEC* capacity, especially in Hg-M4-A and Hg-M4-D in which the *CEC* is not satisfied by Na^{+} and/or Hg^{2+} (Fig. 1). The small intensity of Hg M line in the EDX spectra of Hg-M4-A and Hg-M4-B (Fig. S2) could be explained by this leached Al^{3+} to the interlayer space (Fig. S3).

In general, the ^{29}Si MAS NMR spectra can be described as a wide band in the range between −70 ppm and −95 ppm, associated with $Q^3(mAl)$ with $0 \leq m \leq 3$ environments on phyllosilicates 2:1 (Fig. 4). The differences observed in the spectra (relative intensities and shifts) are due to the different quantity of $Q^3(mAl)$ sites expected in the micas (Alba et al., 2006; Pavón et al., 2014).

In the X-M4 (Fig. 4), ^{29}Si peaks shift to lower frequency values when the ionic radius of the cations increases (lower hydrated radius). In the samples with the lowest layer charge, this displacement is also shown, but it is smaller than in the highest charged mica, due to the lower cations concentration in the interlayer space.

The exchanged reaction causes changes in the relative intensity of the signals and a line broadening of the ^{29}Si MAS NMR signals, similar to that observed in the tetrahedral ^{27}Al MAS NMR signal (Fig. S3), probably due to the distortion exerted on the tetrahedral Si^{4+} as consequence of the location of the interlayer cation in the pseudohexagonal cavity

(Alvero et al., 1994). In Hg-M4-D, the signal of ϒ-ringwoodite at -81.3 ppm, (Stebbins et al., 2009) observed by XRD, overlaps with the ^{29}Si signals of mica.

A d_{001} value of 1.22 nm implies an estimated interlayer space height of 0.26 nm and as the Van der Waal diameter of water is 0.28 nm (Finney, 2001), a steric effect has to be considered to accommodate the fully hydrated cation in the middle of the interlayer space. Therefore, the cations trend to form an inner complex with the basal oxygen plane that provokes a change of the chemical shift and a broadening line of the ^{29}Si and ^{27}Al MAS NMR signals.

3.1. Effect of the heavy metal initial salt concentration

Comparing A and B samples, the effect of the initial heavy metal concentration, C_0, on the efficiency of the cation exchange reaction can be inferred.

When a higher C_0 is offered (X-M4-B), the amount of desorbed Na^+ and adsorbed X^{2+} increases, indicating that the exchange reaction is favoured (Fig. 1), being the only exception the exchange with Cd^{2+} where nearly the same quantity of metal is adsorbed nevertheless the initial C_0. In this case, the distribution ratio between liquid and solid, K_d, remains constant (60.7 L/kg for Cd-M4-A and Cd-M4-B) and a saturation of the Cd^{2+} active site can be concluded.

XRD data reveals that the crystallinity of the samples is not affected by C_0, and neither the basal space that does not change after increasing the initial heavy metal concentration. However, the exchange reaction with Hg^{2+} produces that at higher C_0 (Hg-M4-B) only one *001* reflection at 1.36 nm is observed whereas in the EDX spectra none Hg M line can be seen. ^{27}Al MAS NMR reveals an increase in the octahedral Al^{3+} signal which is accompanied by a nearly absence of the exchangeable Na^+ signal in the ^{23}Na MAS NMR, thus, indicates the leaching of Al^{3+} and probably H_3O^+ cations are responsible for the

observed basal spacing. Non-change is observed in the local order of the aluminosilicate structure, see ^{29}Si MAS NMR spectra in Fig. 4, with increasing of the initial heavy metal concentration.

3.2. Effect of the counterion

The analysis of the samples of series B and C (Table 1) allows evaluating the effect of the counterion on the efficiency of the cation exchange reaction. Neal and Sposito (Neal and Sposito, 1986) assumed that Cl^- and NO_3^- have weak effect on metal ion adsorption but our results demonstrate that this is not true for high charge swelling micas, where their adsorption ability for heavy metal cations is affected.

Na^+ leaching is favoured in presence of Cl^- (X-M4-B) as reported by Sharma and Sharma (Sharma and Sharma, 2013) who observed that Cl^- anion seems to have promoted alkali cation leaching in comparison with other anionic medium. However, the medium has an unlike behaviour in the heavy metal adsorption: while the adsorption of Cd^{2+} and Hg^{2+} is disfavoured in the presence of Cl^-, the opposite occurred for the Pb^{2+} adsorption. The reason may be the formation of $Pb(OH)_2$ species in the presence of NO_3^-, both the *pH* and E_H conditions in the NO_3^- medium (Fig. S1) favoured this formation, and the formation of complexes with Cl^- in the case of Cd^{2+} and Hg^{2+} that diminish the adsorption (El-Hefnawy et al., 2014; Ugochukwu et al., 2013).

A higher hydration of the layer is observed in the case of Cl^- as counterion in comparison with NO_3^- (Fig. 2). Sato (Sato, 2008) has reported that the water activity on porewater of swelling smectites depends on the counterion, thus, the water content is higher when the counterion is Cl^- instead of NO_3^-. No local order change is observed in the MAS NMR spectra.

3.3. Effect of the mica/heavy metal solution stirring during equilibration

In general, no or minor changes are observed as consequence of the equilibration process between Na-M4 and heavy metal solutions (X-M4-C *vs* X-M4-D). In the case of Pb^{2+} and Cd^{2+}, the adsorbed heavy metal amount is higher in X-M4-D (Fig. 1) as a consequence of the higher quantity offered to the samples. However, the desorbed Na^{+} decreases in X-M4-D (Fig. 1), which infers a lower exchange capacity of Na^{+} by X^{2+}, the exchange reaction being more efficient in X-M4-C. No structural changes are observed as a consequence of the equilibration process.

For Hg^{2+}, the opposite trend is observed, desorbed Na^{+} is higher in Hg-M4-D and adsorbed Hg^{2+} is higher in Hg-M4-C. The high acid reaction medium that provokes a quite high leached Al^{3+} and partially exchanges the interlayer Na^{+} may be the responsible of that behaviour (Fig. S3). No other structural changes are observed as a consequence of the equilibration process.

3.4. Effect of the layer charge

Finally, we focus on structural parameters of the exchangeable material and the influence of the mica layer charge on their ability to exchange their interlayer sodium cations by heavy metals ones is analysed.

The amount of desorbed Na^{+} and absorbed X^{2+} increases when layer charge decreases, indicating that the strong electrostatic attraction between the charged surface of Na-M4 difficults the diffusion of X^{2+} into the interlayer space (Pavón et al., 2014; Pavon et al., 2013). In general, those synthetic micas has higher heavy metal exchange capacity than natural and modified smectites, bentonite, kaolinite or zeolite (Rajec et al., 1999; Uddin, 2017). The only exception was the adsorption of Hg^{2+} on hydroxyapatite that was higher

(Uddin, 2017) (2541.8 meq/kg vs 515 or 1878.5 meq/kg on Hg-M4-D and Hg-M2-D, respectively).

Despite of the different cation exchange capacity of Na-M2 and Na-M4 (2475.25 meq/kg and 4694.84 meq/kg, respectively), the swelling of the layer remains constant (similar d_{001} value, Fig. 2), except for Cd^{2+}. When the layer charge decreases, Na-M2, the position of the *001* reflection of the Cd-M2-D shifts to a lower 2θ value, which corresponds to higher basal space (up to 1.45 nm). This increased layer separation for the Mica-2 is likely to be due to small cations located in a two layer closer to the surface and can adsorb more water molecules (Pavon et al., 2013).

In addition, silicate layer charge also affects the formation of inner sphere complexes. When layer charge increases, the negative charge of the surface also increases, and, therefore, the materials turn out to have more tendency on forming inner sphere complex and the effect of the interlayer cation is more evident, as can be seen in the displacement of the chemical shift and line broadening of the ^{29}Si and ^{27}Al MAS NMR signals (Fig. 4 and Fig. S3).

4. Conclusions

In this contribution, the selectivity for the sodium exchange by heavy metals cations is explored for a series of high charge swelling micas, analysing different experimental conditions. The efficiency of cation exchange and the adsorption mechanism depend on the experimental conditions, but, in general, the maximum adsorption has the trend: Hg^{2+} > Pb^{2+} > Cd^{2+} and is quite higher than in natural and modified clay minerals and the exchange reaction is more efficient when layer charge diminishes. The metal cations are located in the pseudohexagonal cavity as an inner sphere complex which is favoured as the layer charge increases and depends on the physical properties of the heavy metal.

However, the interlayer structure of the hydrated mica is retained during the ion-exchange reaction.

Supporting information

The Supporting Information is available free of charge on the Publications website.

Experimental variables and *pH* of initial and post-exchange reaction solutions. Pourbaix diagram of aqueous solution of metals in the initial solution. EDX spectra of lamellar particles for all the cation exchange conditions. ^{27}Al MAS NMR spectra of Na-M4 and Na-M2 after metal adsorption at different experimental conditions.

Acknowledgements

The authors would like to thank the Junta de Andalucía (Spain) and FEDER (Proyecto de Excelencia de la Junta de Andalucía, project P12-FQM-567), to the Spanish State Program R+D+I oriented societal challenges and FEDER (Project MAT2015-63929-R) for financial support. F.J. Osuna thanks his grant to the training researcher program associated to the excellence project of Junta de Andalucía (P12-FQM-567).

Table S1

Cation exchange conditions (X=Pb^{2+}, Cd^{2+}, Hg^{2+})

	counterion	C_0 (meq/l)	L/S (ml/g)	Total C_0 (meq/kg)	stirring
X-M4-A	Cl^-	35.3	50	7042.3	magnetic
X-M4-B	Cl^-	47	50	9389.7	magnetic
X-M4-C	NO_3^-	47	50	9389.7	magnetic
X-M4-D	NO_3^-	47	200	38779.4	end-over
X-M2-D	NO_3^-	24.8	200	19802.0	end-over

CEC (Na-M2)= 2475.25 meq/kg and *CEC* (Na-M4)= 4694.84 meq/kg

Table 2

Physicochemical properties of heavy metals[a]

	Pb^{2+}	Cd^{2+}	Hg^{2+}
r (Å)	1.19	0.95	1.02
η	8.46	10.29	7.70
pK_H	7.70	10.01	3.40

[a]r represents the effective ionic radius, η represents the hardness and pK_H is the hydrolysis constant.

FIGURE CAPTION

Fig. 1. X^{2+} sorption parameters on X-M*n* (*n*=2 and 4). The dash lines mark the *CEC* of the Na-M*n*.

Fig. 2. XRD of X-M*n* at different experimental conditions (X=Pb^{2+}, Cd^{2+} or Hg^{2+} and *n*=2 or 4). *=PbCl(OH) PDF 04-011-5179; o=$PbO{\cdot}4H_2O$ PDF 00-018-0701 or HgO PDF 04-007-4740; f=PbF_2 PDF 04-005-4701; h=$Hg(NO_3)_2{\cdot}3H_2O$ PDF 00-031-0855; e=spinel ($MgAl_2O_4$) PDF 04-006-9814; +=MgO PDF 01-080-4193; ^=Ringwoodite ϒ-Mg_2SiO_4 PDF 01-077-8396

Fig. 3. ^{23}Na MAS NMR spectra of X-M*n* at different experimental conditions (X=Pb^{2+}, Cd^{2+} or Hg^{2+} and *n*=4 or 2).

Fig. 4. ^{29}Si MAS NMR spectra of X-M*n* at different experimental conditions (X=Pb^{2+}, Cd^{2+} or Hg^{2+} and *n*=4 or 2).

Fig. 1

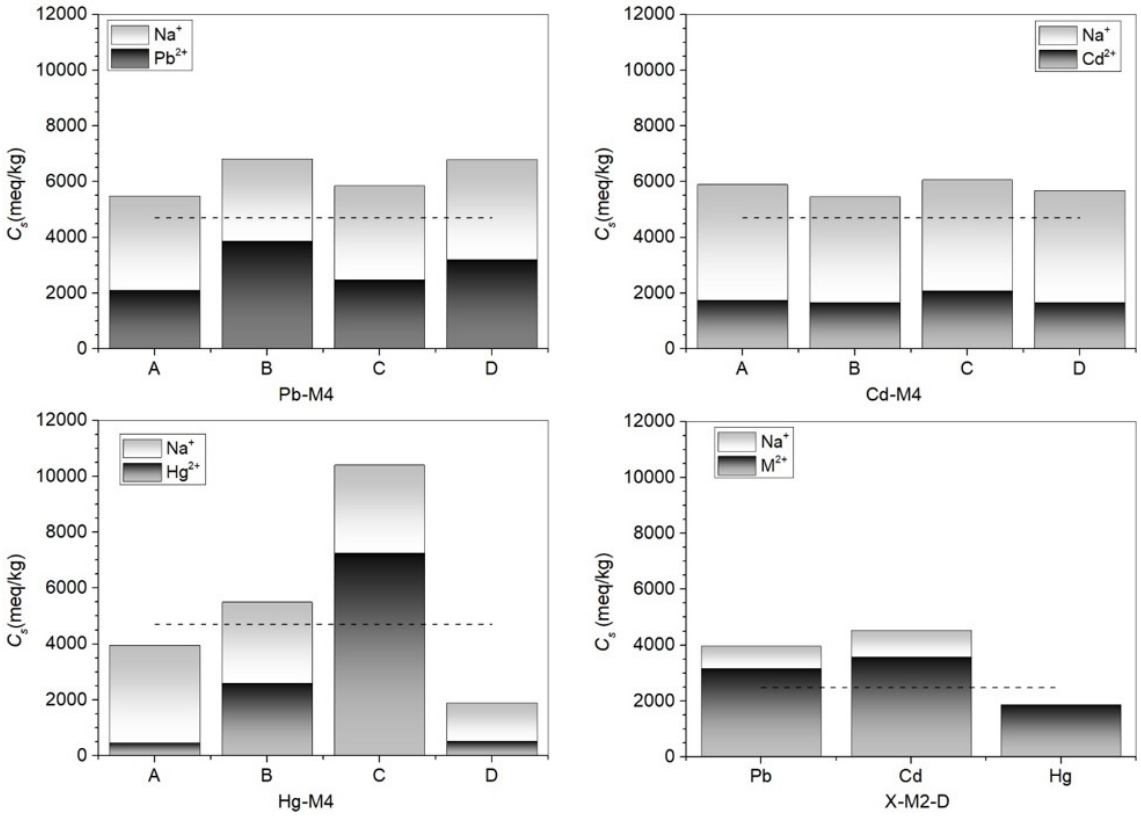
Na+
Pb2+
Cs (meq/kg)
12000
10000
8000
6000
4000
2000
0
A
B
C
D
Pb-M4
Na+
Cd2+
Cd-M4
Na+
Hg2+
Hg-M4
Na+
M2+
Pb
Cd
Hg
X-M2-D

Fig. 2

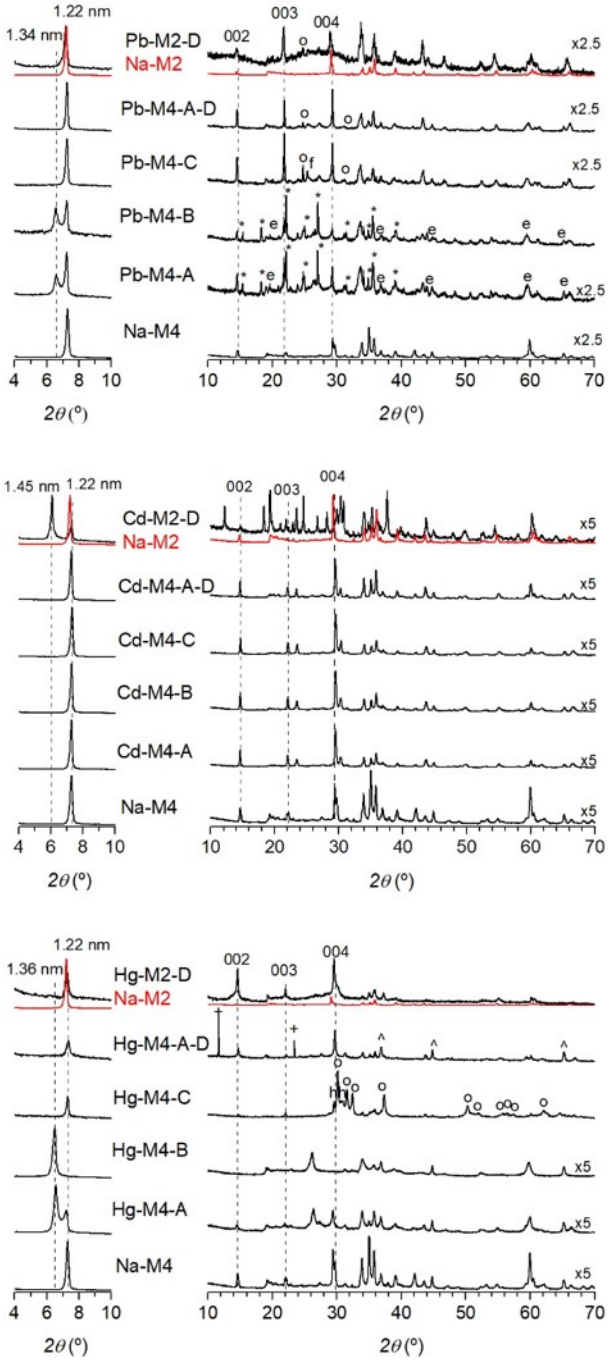
1.22 nm
1.34 nm
Pb-M2-D
Na-M2
Pb-M4-A-D
Pb-M4-C
Pb-M4-B
Pb-M4-A
Na-M4
002
003
004
x2.5
2θ(°)
1.45 nm
1.22 nm
Cd-M2-D
Na-M2
Cd-M4-A-D
Cd-M4-C
Cd-M4-B
Cd-M4-A
Na-M4
x5
1.36 nm
Hg-M2-D
Na-M2
Hg-M4-A-D
Hg-M4-C
Hg-M4-B
Hg-M4-A
Na-M4

Fig. 3

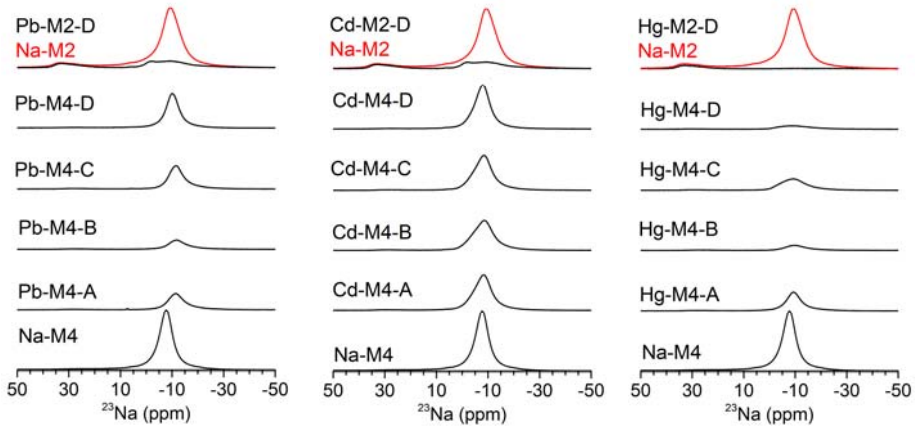
Pb-M2-D
Na-M2
Pb-M4-D
Pb-M4-C
Pb-M4-B
Pb-M4-A
Na-M4
Cd-M2-D
Na-M2
Cd-M4-D
Cd-M4-C
Cd-M4-B
Cd-M4-A
Na-M4
Hg-M2-D
Na-M2
Hg-M4-D
Hg-M4-C
Hg-M4-B
Hg-M4-A
Na-M4
50 30 10 -10 -30 -50
23Na (ppm)

Fig. 4

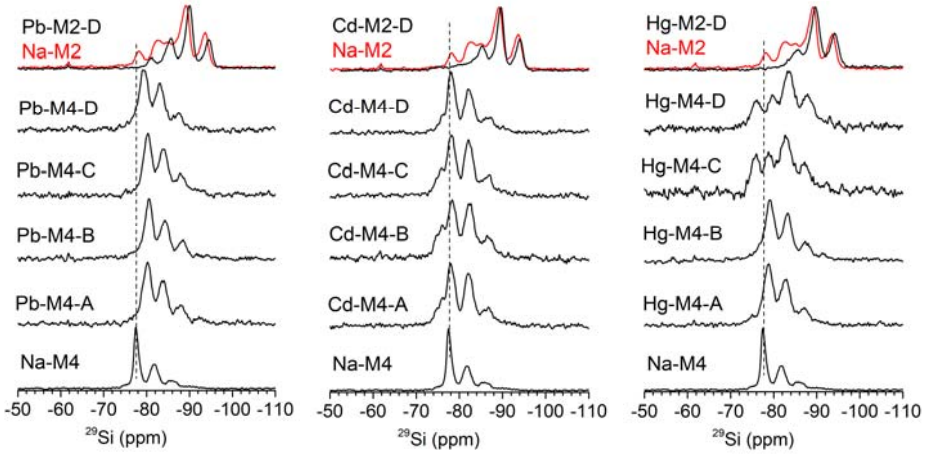
Pb-M2-D
Na-M2
Pb-M4-D
Pb-M4-C
Pb-M4-B
Pb-M4-A
Na-M4
Cd-M2-D
Na-M2
Cd-M4-D
Cd-M4-C
Cd-M4-B
Cd-M4-A
Na-M4
Hg-M2-D
Na-M2
Hg-M4-D
Hg-M4-C
Hg-M4-B
Hg-M4-A
Na-M4
-50 -60 -70 -80 -90 -100 -110
29Si (ppm)

GRAPHICAL ABSTRACT

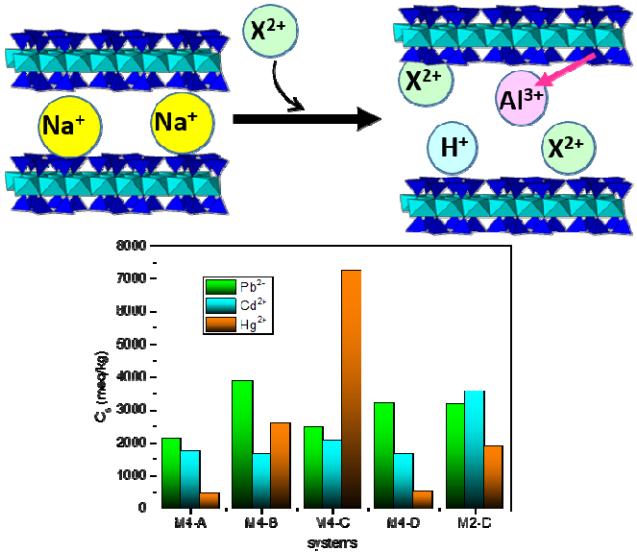

References

Al-Saleh, I., Coskun, S., Mashhour, A., Shinwari, N., El-Doush, I., Billedo, G., Jaroudi, K., Al-Shahrani, A., Al-Kabra, M., Mohamed, G.E.D., 2008. Exposure to heavy metals (lead, cadmium and mercury) and its effect on the outcome of in-vitro fertilization treatment. Int. J. Hyg. Environ. Health 211, 560-579.

Alba, M.D., Becerro, A.I., Castro, M.A., Perdigon, A.C., 2001a. Hydrothermal reactivity of Lu-saturated smectites: Part I. A long-range order study. Am. Miner. 86, 115-123.

Alba, M.D., Becerro, A.I., Castro, M.A., Perdigon, A.C., 2001b. Hydrothermal reactivity of Lu-saturated smectites: Part II. A short-range order study. Am. Miner. 86, 124-131.

Alba, M.D., Castro, M.A., Naranjo, M., Pavon, E., 2006. Hydrothermal reactivity of Na-n-micas (n=2, 3, 4). Chem. Mat. 18, 2867-2872.

Alvero, R., Alba, M.D., Castro, M.A., Trillo, J.M., 1994. Reversible migration of lithium in montmorillonites. J. Phys. Chem. 98, 7848-7853.

Churchman, G.J., Gates, W.P., Theng, B.K.G., Yuan, G., 2006. Chapter 11.1 Clays and Clay Minerals for Pollution Control, in: Bergaya, F., Theng, B.K.G., Lagaly, G. (Eds.), Developments in Clay Science. Elsevier, pp. 625-675.

El-Hefnawy, M.E., Selim, E.M., Assaad, F.F., Ismail, A.I., 2014. The Effect of Chloride and Sulfate Ions on the Adsorption of Cd^{2+} on Clay and Sandy Loam Egyptian Soils. Sci. World J., 6.

Finney, J.L., 2001. The water molecule and its interactions: the interaction between theory, modelling, and experiment. J. Mol. Liq. 90, 303-312.

Fu, F.L., Wang, Q., 2011. Removal of heavy metal ions from wastewaters: A review. J. Environ. Manage. 92, 407-418.

Garcia-Jimenez, M.J., Cota, A., Osuna, F.J., Pavon, E., Alba, M.D., 2016. Influence of temperature and time on the Eu^{3+} reaction with synthetic Na-Mica-n (n=2 and 4). Chem. Eng. J. 284, 1174-1183.

Gonzalez-Davila, M., Santana-Casiano, J.M., Millero, F.J., 2007. Use of pitzer equations to examine the formation of Mercury(II) hydroxide and chloride complexes in $NaClO_4$ media. Aquat. Geochem. 13, 339-355.

Jimenez-Castaneda, M.E., Medina, D.I., 2017. Use of Surfactant-Modified Zeolites and Clays for the Removal of Heavy Metals from Water. Water 9.

Kang, S.Y., Lee, J.U., Moon, S.H., Kim, K.W., 2004. Competitive adsorption characteristics of Co^{2+}, Ni^{2+}, and Cr^{3+} by IRN-77 cation exchange resin in synthesized wastewater. Chemosphere 56, 141-147.

Kim, H.N., Ren, W.X., Kim, J.S., Yoon, J., 2012. Fluorescent and colorimetric sensors for detection of lead, cadmium, and mercury ions. Chem. Soc. Rev. 41, 3210-3244.

Kodama, T., Komarneni, S., 1999. Na-4-mica: Cd^{2+}, Ni^{2+}, Co^{2+}, Mn^{2+} and Zn^{2+} ion exchange. J. Mater. Chem. 9, 533-539.

Kodama, T., Komarneni, S., Hoffbauer, W., Schneider, H., 2000. Na-4-mica: simplified synthesis from kaolinite, characterization and Zn, Cd, Pb, Cu and Ba uptake kinetics. J. Mater. Chem. 10, 1649-1653.

Kodama, T., Ueda, M., Nakamuro, Y., Shimizu, K., Komarneni, S., 2004. Ultrafine na-4-mica: Uptake of alkali and alkaline earth metal cations by ion exchange. Langmuir 20, 4920-4925.

Matusik, J., Wscislo, A., 2014. Enhanced heavy metal adsorption on functionalized nanotubular halloysite interlayer grafted with aminoalcohols. Appl. Clay Sci. 100, 50-59.

Naranjo, M., Castro, M.A., Cota, A., Osuna, F.J., Pavon, E., Alba, M.D., 2015. Synthesis temperature effect on Na-Mica-4 crystallinity and heteroatom distribution. Micropor. Mesopor. Mat. 204, 282-288.

Neal, R.H., Sposito, G., 1986. Effects of soluble organic-matter and sewage-sludge amendments on cadmium sorption by soils at low cadmium concentrations. Soil Science 142, 164-172.

O'Connell, D.W., Birkinshaw, C., O'Dwyer, T.F., 2008. Heavy metal adsorbents prepared from the modification of cellulose: A review. Bioresour. Technol. 99, 6709-6724.

Park, M., Kim, H.J., Kim, K.S., Duckworth, O.W., Komarneni, S., 2012. Hydronium-Promoted Equilibrium Mechanism for the Alkali Metal Cation Exchange Reaction in Na-4-Mica. J. Phys. Chem. C 116, 18678-18683.

Pavón, E., Castro, M.A., Cota, A., Osuna, F.J., Pazos, M.C., Alba, M.D., 2014. Interaction of Hydrated Cations with Mica-n (n = 2, 3 and 4) Surface. J. Phys. Chem. C 118, 2115-2121.

Pavon, E., Castro, M.A., Naranjo, M., Orta, M.M., Pazos, M.C., Alba, M.D., 2013. Hydration properties of synthetic high-charge micas saturated with different cations: An experimental approach. Am. Miner. 98, 394-400.

Pavon, E., Osuna, F.J., Alba, M.D., Delevoye, L., 2014. Direct evidence of Lowenstein's rule violation in swelling high-charge micas. Chem. Commun. 50, 6984-6986.

Pazos, M.C., Castro, M.A., Cota, A., Osuna, F.J., Pavon, E., Alba, M.D., 2017. New insights into surface-functionalized swelling high charged micas: Their adsorption performance for non-ionic organic pollutants. J. Ind. Eng. Chem. 52, 179-186.

Pearson, R.G., 1988. Absolute electronegativity and hardness - application to inorganic-chemistry. Inorg. Chem. 27, 734-740.

Persson, I., 2010. Hydrated metal ions in aqueous solution: How regular are their structures? Pure Appl. Chem. 82, 1901-1917.

Rajec, P., Macasek, F., Misaelides, P., 1999. Sorption of heavy metals and radionuclides on zeolites and clays, in: Misaelides, P., Macasek, F., Pinnavaia, T.J., Colella, C. (Eds.), Natural Microporous Materials in Environmental Technology, pp. 353-363.

Sanz, J., Serratosa, J.M., 1984. Si-29 and Al-27 high-resolution MAS-NMR spectra of phyllosilicates. J. Am. Chem. Soc. 106, 4790-4793.

Sato, H., 2008. Thermodynamic model on swelling of bentonite buffer and backfill materials. Phys. Chem. Earth 33, S538-S543.

Sharma, V., Sharma, K.N., 2013. Influence of Accompanying Anions on Potassium Retention and Leaching in Potato Growing Alluvial Soils. Pedosphere 23, 464-471.

Srinivasan, R., 2011. Advances in Application of Natural Clay and Its Composites in Removal of Biological, Organic, and Inorganic Contaminants from Drinking Water. Advances in Materials Science and Engineering.

Stebbins, J.F., Panero, W.R., Smyth, J.R., Frost, D.J., 2009. Forsterite, wadsleyite, and ringwoodite (Mg_2SiO_4): Si-29 NMR constraints on structural disorder and effects of paramagnetic impurity ions. Am. Miner. 94, 626-629.

Syrmanova, K., Suleimenova, M.T., Sarypbekova, N.K., Botabaev, N.E., Kaldybekova, J.B., 2016. Research of Porization and Adsorptions in High-Porous Adsorptive Layers of Vermiculite. Orient. J. Chem. 32, 1319-1328.

Takahashi, Y., Tada, A., Shimizu, H., 2004. Distribution pattern of rare earth ions between water and montmorillonite and its relation to the sorbed species of the ions. Anal. Sci. 20, 1301-1306.

Uddin, M.K., 2017. A review on the adsorption of heavy metals by clay minerals, with special focus on the past decade. Chem. Eng. J. 308, 438-462.

Ugochukwu, N., Mohamed, I., Ali, M., Iqbal, J., Fu, Q.L., Zhu, J., Jiang, G.J., Hu, H.Q., 2013. Impacts of inorganic ions and temperature on lead adsorption onto variable charge soils. Catena 109, 103-109.

Yuan, G., 2004. Natural and Modified Nanomaterials as Sorbents of Environmental Contaminants. J. Environ. Sci. Health., Part A 39, 2661-2670.

Yuan, G.D., Theng, B.K.G., Churchman, G.J., Gates, W.P., 2013. Chapter 5.1 - Clays and Clay Minerals for Pollution Control, in: Bergaya, F., Lagaly, G. (Eds.), Developments in Clay Science. Elsevier, pp. 587-644.

Zhu, R., Zhou, Q., Zhu, J., Xi, Y., He, H., 2015. Organo-clays as sorbents of hydrophobic organic contaminants: Sorptive characteristics and approaches to enhancing sorption capacity. Clay Clay Min. 63, 199-221.